Title: Why do continental normal fault earthquakes have smaller maximum magnitudes?

Authors: James S. Neely[1,2], Seth Stein[1,2]

Affiliations:

1. Department of Earth and Planetary Science, Northwestern University, 2145 Sheridan Road, Evanston, IL, 60208
2. Institute for Policy Research, Northwestern University, 2040 Sheridan Road, Evanston, IL, 60208

Corresponding Author:

James S. Neely – james@earth.northwestern.edu

Abstract:
Continental normal fault earthquakes have been reported to have smaller maximum magnitudes (M_{max}) than continental earthquakes with other fault geometries. This difference has significant implications for understanding seismic hazards in extensional regions. Using the Global Centroid Moment Tensor (GCMT) catalog, we examine how M_{max} varies with fault geometry in continental regions, whether these trends are robust, and potential physical reasons for the smaller magnitudes of continental normal fault earthquakes.

We find that the largest continental normal fault earthquakes are in the low M_w 7 range whereas other fault geometries can reach ~M_w 8. The continental normal fault earthquake magnitude-frequency distribution has a lower corner magnitude (a parameterization of M_{max}) than other fault geometries. The observed smaller continental normal fault M_{max} is not an artifact of classification criteria or catalog length. Probability calculations indicate that the GCMT catalog is long enough to capture differences in M_{max} due to fault geometry. Additionally, our analysis indicates that neither fault length nor width is limiting the size of continental normal fault earthquakes. Fault complexity can limit rupture extent, but it is likely not the primary reason for the smaller continental normal fault M_{max}.

Rather, lithosphere yield stress (strength) appears to be the main factor controlling M_{max}. In extension, lithosphere is weaker, failing at lower yield stresses than in compression. Although this yield stress difference is consistent with smaller continental normal fault earthquakes, it appears inconsistent with the occurrence of large oceanic normal fault earthquakes. However, the largest oceanic normal fault earthquakes occur near subduction zones where the lithosphere is bending. Laboratory studies indicate that bending lithosphere likely has a higher yield stress than lithosphere in pure extension, which may allow for larger oceanic normal fault earthquakes. Therefore, yield stress—rather than fault geometry alone—appears to be the key factor limiting an earthquake's maximum magnitude.

Key words: Continental earthquakes, maximum magnitude, normal fault earthquakes

1.1 Introduction

How fault geometry influences an earthquake's maximum magnitude (M_{max}) is important for understanding seismic hazards. In continental regions, it is commonly assumed that the largest normal fault earthquakes are smaller than those of other fault geometries (Jackson and White, 1989). Some of the largest historical continental strike-slip and thrust earthquakes include the 1906 M_w 7.9 San Francisco (Biasi et al., 2013), 1911 M_w 8.0 Chon-Kemin, Kazakhstan (Kulikova and Krüger, 2015), 1920 M_w 8.0 Haiyuan, China (Deng et al., 1984), 1957 M_w 8.1 Gobi-Altai, Mongolia (Okal, 1976), 1990 M_w 7.7 Luzon, Philippines (Velasco et al., 1996), 2002 M_w 7.8 Denali, Alaska (Ekström et al., 2012), and 2008 M_w 7.9

Wenchuan, China earthquakes (Yu et al., 2010). These are much larger than the largest historical normal fault earthquakes, which include the 1887 M_w 7.5 Sonora, Mexico (Suter, 2015), 1915 M_w 7.3 Pleasant Valley, Nevada (Wesnousky, 2008), 1954 M_w 7.1 Fairview Peak, Nevada (Doser, 1986), and 1959 M_w 7.3 Hebgen Lake, Montana (Doser, 1985) earthquakes.

The past 100+ years of earthquake observations suggest that continental normal fault earthquakes have a smaller M_{max}. Whether this observation reflects a fundamental limitation on their size, however, remains unresolved. This question has serious ramifications for seismic hazard in extensional regions. The expected hazard of large normal fault systems, like the 370-km-long Wasatch Fault, changes depending on whether the fault ruptures in single or multiple segments (DuRoss et al., 2016). Likewise, the expected hazard posed by low angle normal faults, which are widespread in extensional regions (Collettini, 2011) but rarely host large earthquakes (Wernicke, 1995; Axen, 1999), strongly depends on whether very large continental normal fault earthquakes will occur.

Before continuing, we should clarify the meaning of M_{max}. M_{max} can either be a "hard" or "soft" cutoff value (Kagan, 2002). Under a "hard" M_{max} framework, it is assumed that no earthquakes can exceed M_{max}. However with a "soft" M_{max}, earthquakes can exceed M_{max} but they are far less likely to occur than we would expect. It is helpful to think of these "hard" and "soft" M_{max} differences in terms of the Gutenberg-Richter earthquake magnitude-frequency relationship. For a "hard" M_{max}, the Gutenberg-Richter curve abruptly terminates at M_{max}, above which no earthquakes are predicted. For a "soft" M_{max}, larger magnitude earthquakes are possible, but their frequency is significantly lower than predicted by the unrestricted Gutenberg-Richter curve. In this paper, M_{max} refers to a "soft" M_{max}.

Here, we examine the observation that continental normal fault earthquakes have a smaller M_{max} than other continental fault geometries. We explore whether these lower magnitudes are an artifact of how we classify earthquakes or relatively short catalog lengths, and (if the observation proves true) potential physical reasons for the smaller magnitudes.

2.1 Data set and earthquake classifications

We use the Global Centroid Moment Tensor (GCMT) catalog (Dziewonski et al., 1981; Ekström et al., 2012) from its inception in 1976 through the end of 2019 to examine how earthquake magnitudes vary with fault geometry. Although the catalog includes earthquakes smaller than moment magnitude (M_w) 5, it is only complete down to M_w 5.8 (Kagan, 2003). We group earthquakes into fault geometry classifications - normal, strike-slip, thrust, and oblique – using Frohlich's (1992) classification based on the plunge of the P, T, and B axes of the earthquake's moment tensor. In this classification, normal earthquakes have a P-axis plunge greater than 60°.

We further divide the earthquakes into six categories by depth and tectonic environment. We classify earthquakes as shallow (≤40 km) or deep (40 - 200 km) and either continental, oceanic, or convergent. These tectonic zone classifications are based on lithosphere type and proximity to a convergent plate boundary. For our purposes, convergent plate boundary earthquakes occur in island arcs, close to (< 20 km) or below the surface of the subducting slab, or in continental lithosphere within 100 km of a convergent plate boundary. Continental earthquakes are those within continental lithosphere that do not meet the convergent criteria. Oceanic earthquakes occur within oceanic lithosphere and do not meet either the convergent or continental criteria. In addition to continental interiors, our definition of continental lithosphere includes continental shelves as well as complex tectonic regions like the Aegean Sea and maritime Southeast Asia.

We classify the earthquakes using a slightly modified version of Matthews et al.'s (2016) island arc and continental polygons. Unlike in the Matthews et al. (2016) dataset, we classify the full Aleutian Islands chain, Japan, and the Okinawa Trough as island arcs. Additionally, we reclassify the Sea of Japan and portions of the Bering Sea as oceanic lithosphere. For convergent boundary earthquakes, we use the USGS's SeismoTectonic Regime Earthquake Calculator (STREC) to calculate the depth to the subducting slab and Coffin et al.'s (1998) dataset to determine distance to a convergent boundary. Table 1

shows the number of shallow earthquakes (the earthquakes of interest here) by fault geometry and tectonic environment with $M_w \geq 5.8$.

Tectonic Environment	Normal	Thrust	Strike-Slip	Oblique	Total
Shallow Continental	135	267	321	162	885
Shallow Oceanic	366	235	1251	158	2010
Shallow Subduction	212	2329	443	441	3425

Table 1: Numbers of earthquakes $M_w \geq 5.8$ in the GCMT database classified by tectonic environment and fault geometry.

3.1 Global distribution of large normal fault earthquakes

Large normal fault earthquakes occur in various tectonic environments. Figure 1 shows all $M_w \geq 6.5$ normal fault earthquakes shallower than 200 km in the GCMT catalog. Most great ($M_w \geq 8$) normal fault earthquakes occur near subduction zones, some within the subducted plate (Okuwaki, and Yagi, 2017). These larger normal fault earthquakes occur due to bending (flexural) stresses within the subducting plate between the trench and outer rise (Craig et al., 2014). Although spreading ridges have numerous small normal fault earthquakes, $M_w \geq 6.5$ earthquakes are rare there. The 1983 Chagos Archipelago earthquake is the largest oceanic earthquake not located near a trench. However, this earthquake may not be as large as it appears to be. Although the GCMT catalog indicates M_w = 7.7, the U.S Geological Survey's (USGS) National Earthquake Information Center (NEIC) lists a lower value of M_w = 7.3.

Shallow continental normal fault earthquakes in the GCMT catalog, on the other hand, rarely exceed M_w 7. The largest normal fault earthquakes occur in extensional plate boundary zones like the Basin and Range province in the western U.S., Italy, eastern Mediterranean, and the East Africa Rift extension zones. Since 1976 (the start of the GCMT catalog), the largest normal fault earthquakes in these regions range from M_w 6.5 to M_w 7.1. Surprisingly, the Baikal Rift in Siberia has no large normal fault earthquakes during this time period. Another conspicuously quiet region is the Basin and Range province in the western U.S. Only one earthquake $\geq M_w$ 6.5 appears in the GCMT catalog (1983 M_w 6.9

Borah Peak, Idaho), although this region hosted large earthquakes ≥ M_w 7 earlier in the 20th century. Figure 2, showing the depth versus magnitude of normal fault earthquakes, highlights the lack of large shallow continental normal fault earthquakes despite their prevalence near convergent plate boundaries and in oceanic environments.

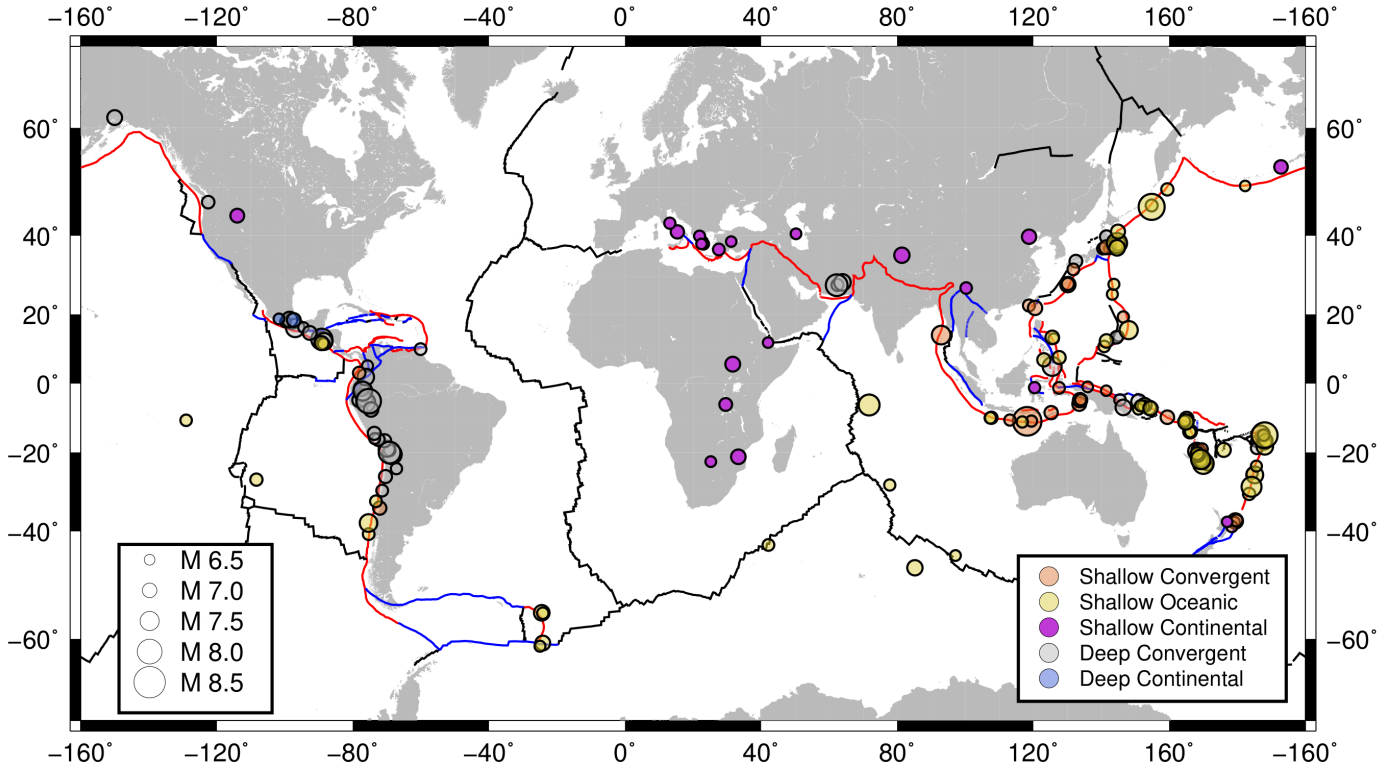

Figure 1: Distribution of $M_w \geq 6.5$ normal fault earthquakes in the GCMT catalog. Circle color corresponds to tectonic environment and depth. Circle size indicates magnitude. Color lines show convergent boundaries (red), spreading centers (black), and transform boundaries (blue) (Coffin et al., 1998). No deep oceanic earthquakes exceed M_w 6.5.

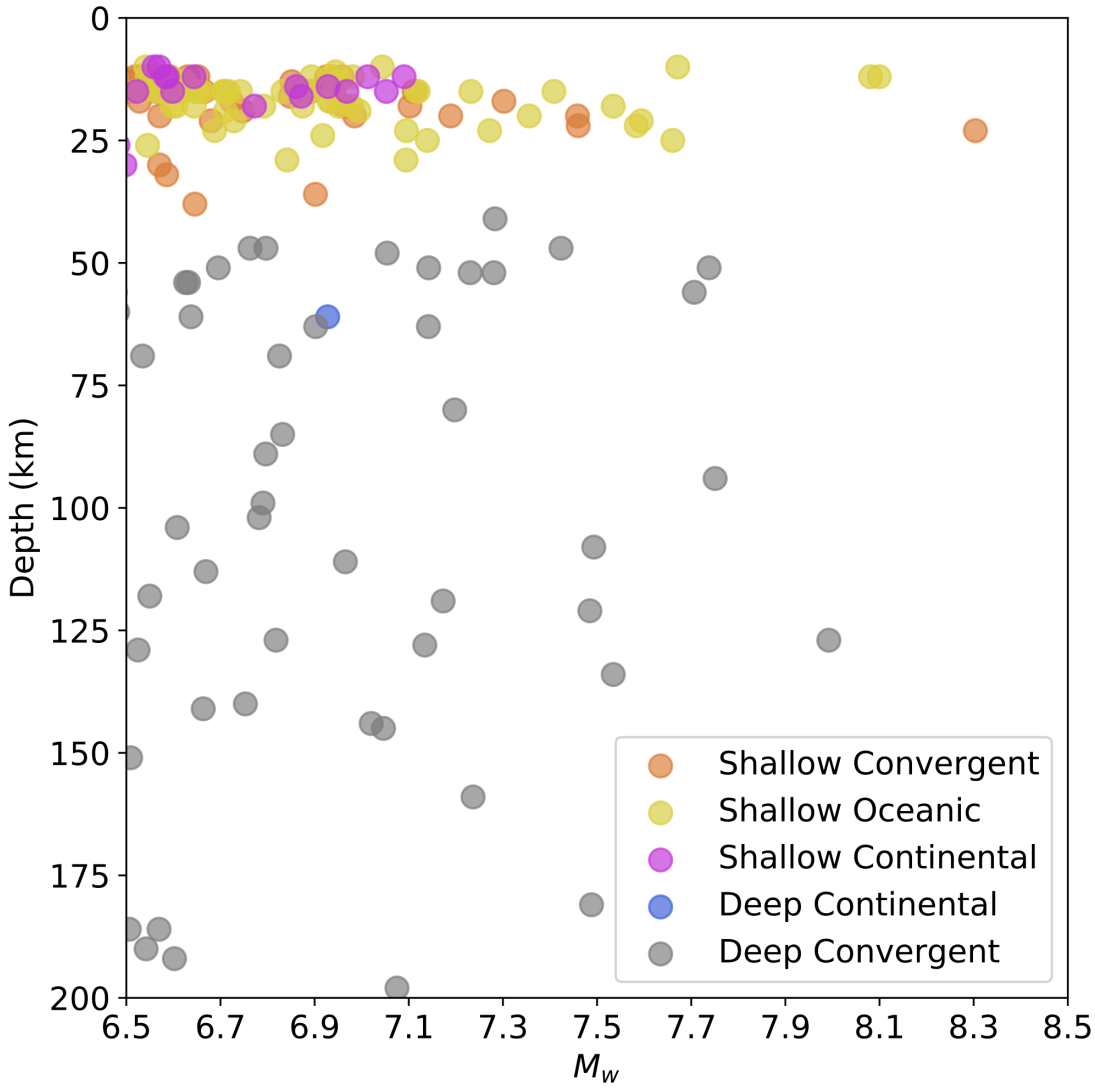

Figure 2: Depth versus magnitude plot for normal fault earthquakes, showing depth and tectonic environment classification. No deep oceanic earthquakes exceed M_w 6.5.

4.1 Variations in earthquake magnitude distribution with fault geometry

The above observations show that over the past 44 years shallow continental normal fault earthquakes rarely exceed M_w 7, although both shallow oceanic and convergent normal fault earthquakes can be much larger. To better understand how fault geometry impacts magnitude, we compare the magnitude distributions of shallow continental, oceanic, and convergent earthquakes (Figure 3). For each fault geometry (normal, thrust, strike-slip, oblique), we fit a tapered Gutenberg-Richter (TGR) distribution using the maximum

likelihood method (Kagan, 2002). The TGR distribution includes two key parameters: *b*-value and corner magnitude (M_c). The *b*-value corresponds to the slope of the cumulative magnitude distribution line. M_c is one specific parameterization of the "soft" M_{max} concept (Kagan, 2002). The inclusion of M_c causes the distribution for larger magnitudes to deviate below the straight line assumed in a traditional unrestricted Guttenberg-Richter distribution. Although various hypotheses have been proposed for what *b*-value (Rundle, 1989) and corner magnitude (Okal and Romanowicz, 1994) physically represent, we simply use these values to parameterize the magnitude distribution curve. Previous studies noted that normal fault earthquakes have a higher *b*-value (Schorlemmer et al., 2005) and that M_c trends can differ between tectonic environments (Kagan, 2002).

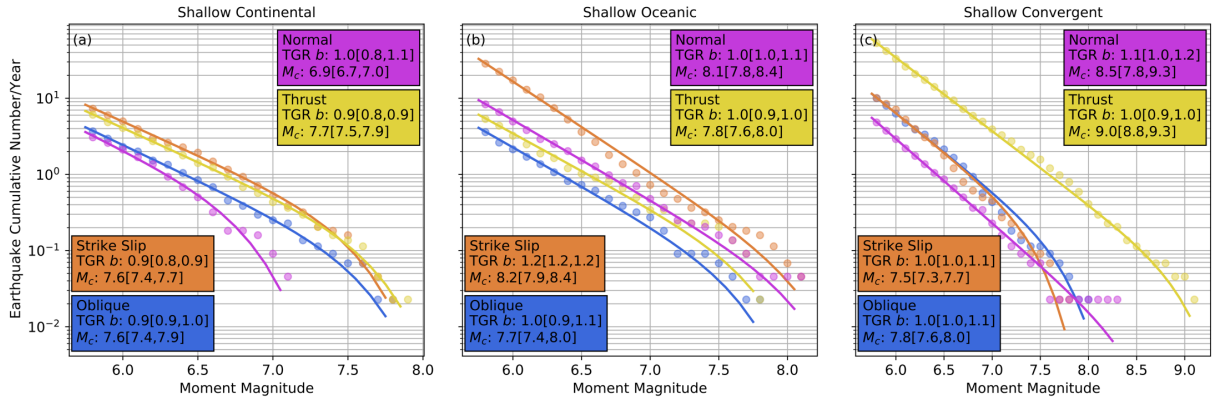

Figure 3: Tapered Gutenberg-Richter distributions for shallow continental (a), oceanic (b), and convergent (c) earthquakes. Color corresponds to earthquake fault geometry with *b*-values and M_c listed for each fault geometry. 1-sigma range indicated for each parameter.

The greatest differences between normal fault earthquakes and other geometries occur for shallow continental earthquakes. For this environment, normal fault earthquakes have the lowest M_c (6.9) compared to the other geometries (Figure 3a) but a similar *b*-value. Thrust, strike-slip, and oblique geometries have an M_c between 7.6 and 7.7. The more earthquakes in the dataset that exceed M_c, the better constrained the estimate of M_c (Kagan, 2002). In the shallow continental environment, the normal fault M_c is best constrained with seven earthquakes exceeding it (Figure 3a). The other fault geometries have at most one or two earthquakes exceeding their M_c.

Normal fault earthquake distributions do not stand out in shallow oceanic (Figure 3b) or shallow convergent (Figure 3c) environments. In shallow oceanic environments, normal fault earthquakes have an M_c (8.1) indistinguishable from strike-slip (8.2) and thrust (7.8) geometries, however these are all poorly constrained. In the shallow convergent environment, the *b*-values are all similar, but thrust earthquakes have the highest M_c (9.0), reflecting the large megathrust earthquakes along convergent interfaces. Although normal fault earthquakes have the next highest M_c (8.5), this estimate is poorly constrained. However, the normal fault M_c for convergent earthquakes appears to be higher than the corresponding M_c values for strike-slip and oblique earthquakes, although these are also poorly constrained. Thus, normal fault earthquakes have significantly smaller maximum magnitudes compared to other fault geometries only in shallow continental regions.

5.1 Smaller normal fault M_{max} not due to classification

Our analysis indicates that in the GCMT catalog, shallow continental normal fault earthquakes have smaller maximum magnitudes. To assess the robustness of this result, we examine how fault geometry classification impacts our assessment of M_{max}. The hard cutoffs in Frohlich's (1992) classification cause similar earthquakes just above and below the cutoff to be grouped separately. In this classification, normal-fault-like earthquakes with P-axis plunges just below 60° are classified as oblique. If the smaller continental normal fault M_{max} observation is robust, oblique earthquakes just below the cutoff should have a similar M_{max} to those above the cutoff.

A plot of magnitude versus P-axis plunge (Figure 4a) shows that oblique earthquakes just below the 60° cutoff are no bigger than those above it. Shallow continental earthquakes (Figure 4a) show a clear pattern in maximum magnitude as P-axis plunge increases from 0° to 90°. Maximum magnitudes approach M_w 8 for strike-slip, thrust, and oblique earthquakes with P-axis plunges less than 50°. Above 50° the largest earthquakes drop to approximately M_w 7 for both normal and oblique geometries. Thus, maximum magnitude drops as the fault geometry becomes more normal-fault like.

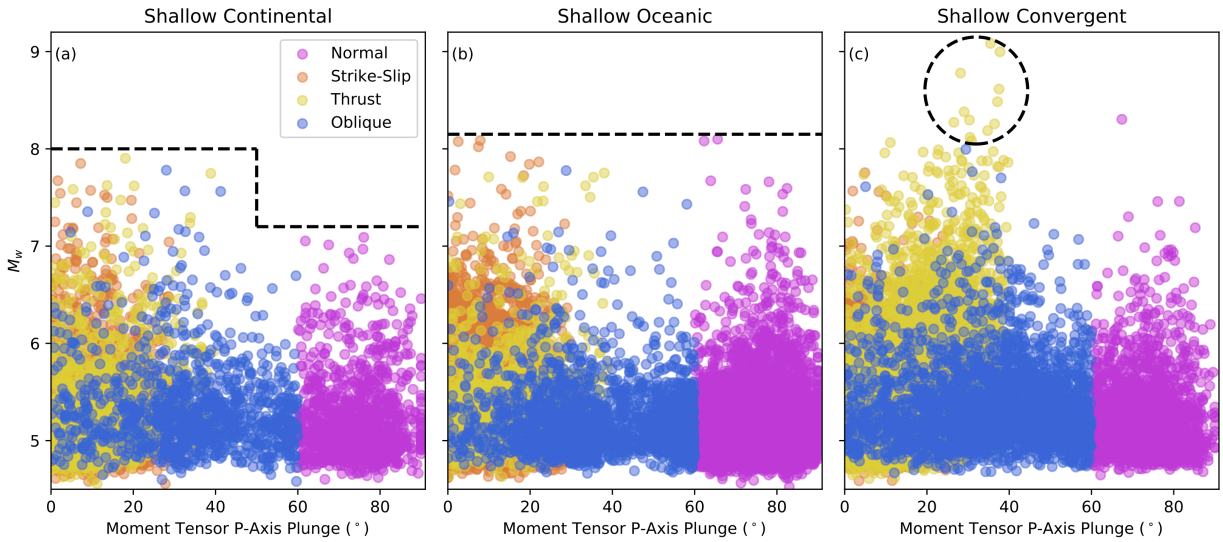

Figure 4: Plot of magnitude versus P-axis plunge for shallow continental (a), oceanic (b), and convergent (c) earthquakes. Circle color corresponds to fault geometry classification. In panel a, the dashed line indicates the drop in M_w with increasing P-axis plunge. In panel b, the dashed line shows constant M_w with increasing P-axis plunge. In panel c, the dashed circle indicates megathrust earthquakes.

We do not observe similar sharp drops in maximum magnitude as the P-axis plunge increases for shallow oceanic (Figure 4b) or shallow convergent (Figure 4c) environments. For shallow oceanic earthquakes, the largest M_w stays relatively constant as P-axis plunge increases. A different M_{max} trend occurs for shallow convergent earthquakes. Instead of a constant M_{max} across the P-axis plunge range, a peak occurs between 30° and 40°, corresponding to megathrust earthquakes at subduction interfaces. Aside from these megathrust earthquakes, the overall trend between M_{max} and P-axis plunge appears flat.

6.1 Smaller normal fault M_{max} not due to catalog length

In the GCMT catalog, shallow continental normal fault earthquakes have a smaller corner magnitude (due to the lack of large earthquakes), but is 44 years long enough to be confident in these differences? We explore this question using probability density functions (PDF) to estimate the likelihood of observing these trends. The tapered Gutenberg-Richter distribution (Figure 3) assumes that the magnitude of each shallow continental normal fault earthquake is independent and drawn from the same PDF (Kagan, 2002). Hence, we can calculate the probability that an earthquake falls within a given magnitude range. By

assuming that the earthquake magnitudes are independent and identically distributed, we can also calculate the probability that a number of earthquakes all fall within the same magnitude range by taking the probability for one earthquake and raising it to a power equal to the number of earthquakes. We can use the same procedure to estimate the probability that no earthquakes exceed a specified magnitude.

The GCMT catalog contains 135 shallow continental normal fault earthquakes with $M_w \geq 5.8$. We calculate the probability that none of 135 such earthquakes would exceed M_w 7.1, the largest in the catalog, for a range of b-values and M_c. A high probability indicates the lack of earthquakes greater than M_w 7.l is a likely outcome. A low probability indicates that it is an unlikely outcome. This lets us assess whether our M_c estimate of 6.9 for shallow continental normal fault earthquakes is reasonable or is artificially low because the GCMT catalog is too short to capture rarer larger events.

The probability estimates show that the catalog is long enough to provide a reasonable estimate of M_c. In Figure 5, the purple lines correspond to the probability that M_w 7.1 is the largest earthquake for three different b-values and a range of M_c values. As M_c increases, the probability that an M_w 7.1 earthquake is the largest in the catalog decreases. For our best estimate of b-value (1.0) and M_c (6.9) there is an ~70% chance that an M_w 7.1 would be the largest earthquake. If we assume a lower b-value (0.8) and higher M_c (7.0) based on the parameters' 1-sigma uncertainties, then the probability decreases to 20%. Conversely, for a higher b-value (1.1) and lower M_c (6.7), the probability is closer to 95%.

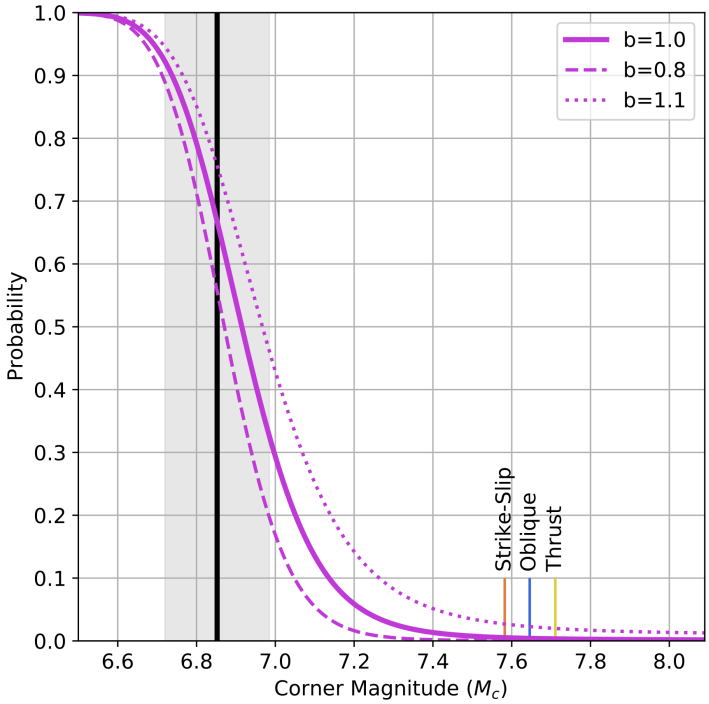

Figure 5: Probability that for 135 earthquakes, M_w 7.1 is the largest observed earthquake for a range of M_c using a tapered Gutenberg-Richter distribution. Purple lines indicate probabilities for different *b*-values. Best estimate of shallow, normal continental M_c (black line) with 1 sigma indicated (grey shading). Corner magnitudes for other fault geometries indicated.

It is highly unlikely that the M_c for shallow continental normal fault earthquakes is as large as the M_c for thrust, strike-slip, and oblique earthquakes, which we estimated to be between 7.6 to 7.7. If normal fault earthquakes had an M_c value to similar to the other fault geometries, there is a less than an approximately 5% chance (and possibly even lower for smaller *b*-values) that the observed M_w 7.1 event would be the largest shallow continental normal fault earthquake. These low probabilities indicate that shallow continental normal fault earthquakes likely have a smaller M_c (and therefore M_{max}) than the other fault geometries, and the GCMT catalog is long enough to observe these differences.

7.1 Reconciling GCMT M_{max} with early instrumental earthquakes

Larger magnitude historical earthquakes that pre-date the GCMT catalog have been reported in extensional environments. However, the lack of a global seismographic network makes it difficult to compare historical instrumental earthquake magnitudes to

284 modern instrumental estimates. Accurate M_w estimates for pre-instrumental earthquakes
285 require well-constrained fault length, width, and slip measurements, but we only directly
286 observe surface rupture length and surface displacement. For instance, the M_w 7.5 estimate
287 for the 1887 Sonora Earthquake is based on the Wells and Coppersmith (1994) empirical
288 scaling relations between surface rupture length and M_w (Suter, 2015). For early
289 instrumental-era earthquakes with few available seismograms like the 1915 Pleasant
290 Valley, Nevada earthquake, discrepancies exist between the M_w 7.3 geologic M_w estimate
291 (Wesnousky, 2008) and instrumental M_w 6.9 to 7.0 estimates (Doser, 1988).
292
293 These historical large extensional environment earthquakes may also contain significant
294 oblique motion (Doser and Yarwood, 1990) resulting in an oblique rather than normal fault
295 classification using the Frohlich (1992) criteria. For instance, the 1910 M_w 7.4 Rukwa
296 earthquake, the largest instrumentally recorded earthquake in East Africa (Ambraseys.
297 1991), appears to have a significant strike-slip component (Ayele and Kulhánek, 2000). The
298 1956 M_w 7.7 Amorgos, Greece earthquake—the largest Aegean Sea earthquake over the
299 past 100 years—may also contain significant oblique motion because some studies find
300 predominantly normal faulting (Okal et al., 2009) whereas others indicate it was primarily
301 strike-slip (Ritsema, 1974). In the Baikal rift region, the largest instrumentally recorded
302 earthquake, the complex 1957 M_w 7.8 Musik earthquake, involved primarily strike-slip
303 faulting (Doser, 1991). The 1959 M_w 7.3 Hebgen Lake, Montana earthquake is another large
304 historical event in an extensional environment with a somewhat complicated geometry.
305 Doser's (1985) body-wave inversion suggests that this earthquake is best described by two
306 subevents, the larger of which contains oblique motion, however the surface rupture
307 indicates predominantly normal faulting displacement (Johnson et al., 2018).
308
309 How do we reconcile the absence of any shallow, normal fault earthquakes with an $M_w >$
310 7.1 in the GCMT catalog with the presence of larger continental normal fault earthquakes in
311 the pre-GCMT instrumental record? Although there is some uncertainty in the moment
312 magnitude and geometry of these early instrumental earthquakes, the 1959 Hebgen Lake,
313 Montana and possibly the 1915 Pleasant Valley, Nevada are M_w 7.3 earthquakes that exceed

the largest GCMT shallow continental normal fault earthquakes. However, the occurrence of these larger magnitude earthquakes is expected given the longer observation window.

If we assume the annual rate of shallow, continental, normal fault earthquakes $\geq M_w$ 5.8 is constant (~3.07 per year based on the GCMT catalog), then we can calculate the probability of observing these larger earthquakes over the length of the historical instrumental record. Figure 6 shows the probability of at least one (Figure 6a), two (Figure 6b), and three (Figure 6c) shallow continental normal fault earthquakes $\geq M_w$ 7.3 occurring in a 120-year span—the approximate length of the historical instrumental catalog (Di Giacomo et al., 2015)—for a range of M_c and b-values. The colors and contours indicate the probability of observing at least 1, 2 or 3 earthquakes $\geq M_w$ 7.3 for a given b-value and M_c combination. The red star and dashed red ellipse indicate the best fitting b-value and M_c and 2-sigma uncertainty ellipse estimated from the GCMT shallow continental normal fault earthquakes.

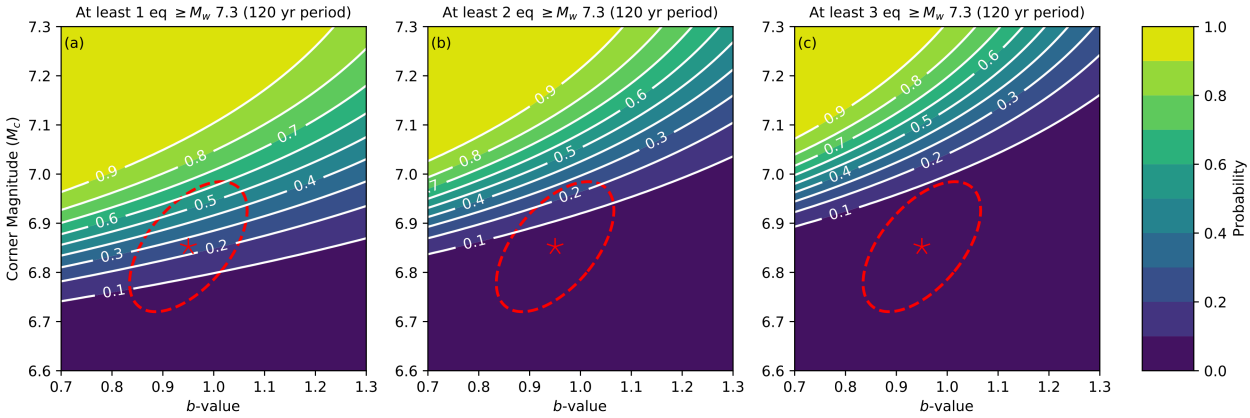

Figure 6: Probability of observing at least 1 (a), 2 (b), or (3) shallow continental normal fault earthquakes $\geq M_w$ 7.3 for a given combination of b-value and M_c over a 120-year period. Colors and contours indicate the probability. The red star and dashed red ellipse indicate the best fitting b-value and M_c and 2-sigma uncertainty ellipse estimated from the GCMT shallow continental normal fault earthquakes.

The probability estimates based on GCMT b-value and M_c parameters seem to be roughly in line with what we observe in the historical instrumental record, but the GCMT-based M_c estimate might be slightly low. The best fitting b-value and M_c parameters indicate that there is a 20% to 30% chance of at least one shallow continental normal fault earthquake $\geq M_w$ 7.3 (1959 Hebgen Lake) in the historical instrumental record (Figure 6a). If we consider the upper end of the 2-sigma uncertainty ellipse, there is an approximately 60%

chance. The probability of at least two earthquakes ≥ M_w 7.3 (1915 Pleasant Valley and 1959 Hebgen Lake) occurring is significantly lower (Figure 6b). The best fitting b-value and M_c parameters indicate less than a 10% chance of at least two earthquakes ≥ M_w 7.3 occurring, but this rises to at least 20% if we consider the upper end of the 2-sigma uncertainty. Although 20% may seem low, it is still a higher probability than rolling a specific number on a 6-sided die. More importantly, due to the tight clustering of the probability contours, a small increase in M_c to 7.0 or 7.1 increases the probability to between 50 and 90%. In the at least three earthquakes ≥ M_w 7.3 scenario (Figure 6c), only a small increase in M_c above the GCMT-based estimate is needed to increase the probability to 50%. Thus an M_c near 7.0 could account for the observed shallow continental normal fault earthquake magnitude distribution over the entire historical instrumental record. A normal fault M_c of 7.0 would still be significantly lower than observed M_c's (7.6-7.7) for thrust, strike-slip, and oblique earthquakes, indicating significant magnitude distribution differences due to fault geometry.

8.1 Fault dimensions not a limitation on normal fault earthquake magnitude

Understanding why shallow continental normal fault earthquakes have a smaller M_{max} has important implications for seismic hazard analysis. Because larger earthquakes require longer faults, fault length may limit the size of normal fault earthquakes. We examine this possibility by comparing the global distribution of extensional faults from the Global Earthquake Model (GEM) Global Active Fault Database (Styron and Pagani, 2020) to the expected surface rupture lengths for normal fault earthquakes (Wells and Coppersmith, 1994).

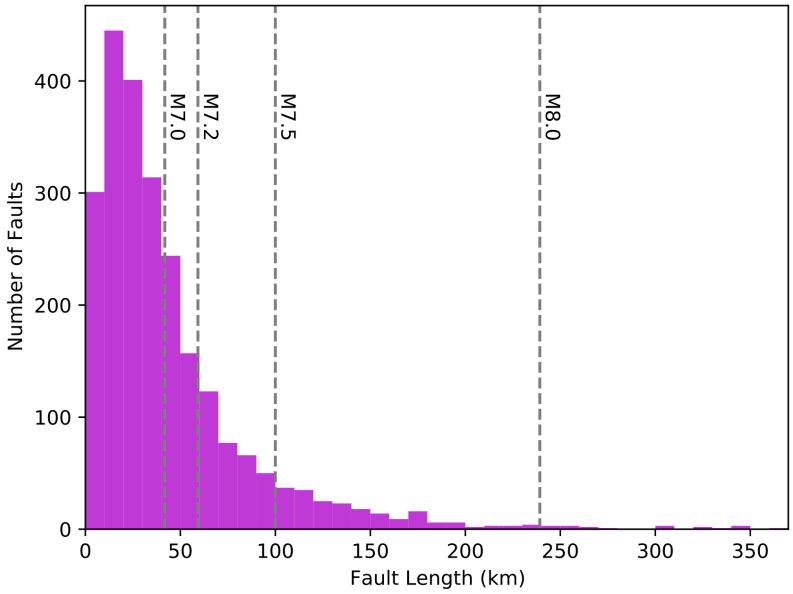

Figure 7: Histogram of active continental normal fault lengths from the GEM-Active Fault database. Vertical lines indicate expected magnitude for the surface rupture length shown (Wells and Coppersmith, 1994).

The fault length histogram (Figure 7) shows that are at least 890 normal faults long enough to host earthquakes $\geq M_w$ 7.0, 547 faults long enough for earthquakes $\geq M_w$ 7.2, 223 faults long enough for earthquakes $\geq M_w$ 7.5, and 22 faults long enough for earthquakes $\geq M_w$ 8.0, especially considering the variability in earthquake rupture length for a given magnitude. Because Wells and Coppersmith's (1994) regression only includes earthquakes with magnitudes from 5.2 to 7.3, it is possible that larger earthquakes do not follow the same relation between fault length and magnitude. However, larger earthquakes generally follow similar trends as smaller earthquakes (Figure 8), but earthquakes with similar magnitudes can have very different surface rupture lengths. Below M_w 7.5, normal fault rupture lengths do not appear to differ significantly from the other two fault geometries, so there is little reason to suggest that larger earthquakes would behave differently.

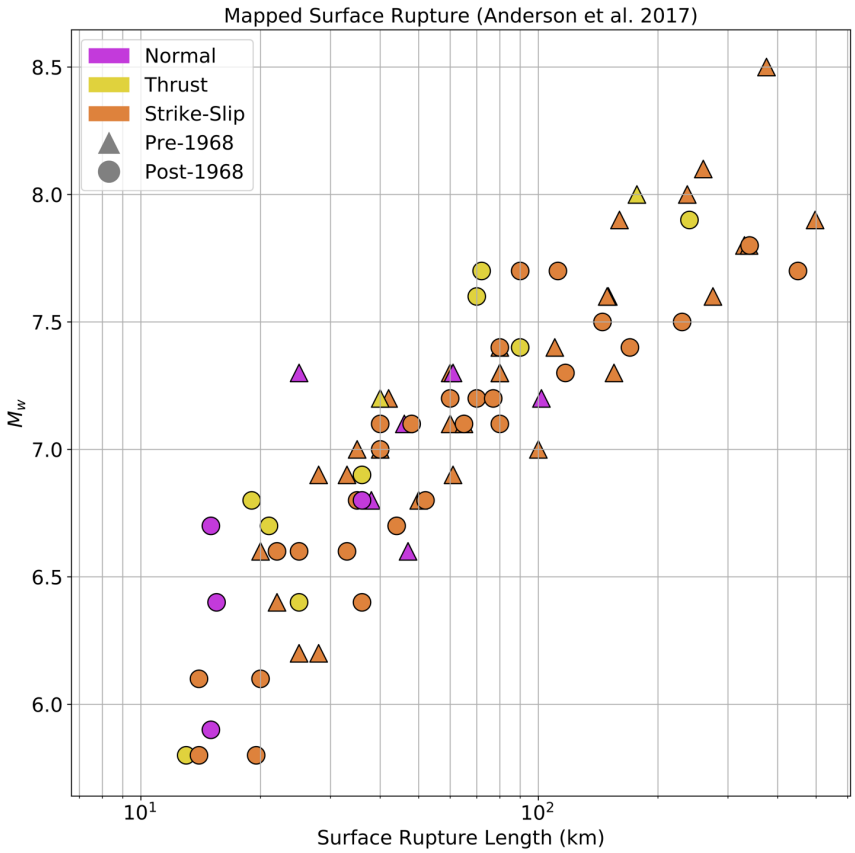

Figure 8: Mapped surface rupture length versus magnitude for large historical earthquakes. Data compiled by Anderson et al. (2017). Color corresponds to geometry. Shape corresponds to earthquake date.

Although the fault length data suggest that some continental normal faults are long enough for larger magnitude earthquakes, the fault database does not indicate how continuous these large faults are. A comprehensive study of normal faults in the Afar region of the East Africa Rift showed that nearly all the faults showed some segmentation regardless of fault length (Manighetti et al., 2015). Fault segmentation is also clearly visible along the Wasatch Fault Zone in Utah and the Fucino Fault Zone in Italy (DuRoss, 2016). Fault segments are delineated by fault gaps, fault branches, fault steps, or changes in fault strike, and it is thought that these complexities limit rupture extent and hence earthquake magnitude (Wesnousky, 1988).

Detailed paleoseismic and historical rupture studies of normal fault earthquakes suggest that fault complexities sometimes, but not always, control rupture extent. A paleoseismic study (DuRoss et al., 2016) found that, along the central portion of the Wasatch Fault Zone, the most recent earthquakes (< 3ka) appear to be confined to individual fault segments. However, older earthquakes may have been multi-segment ruptures. Historical earthquake fault rupture studies also suggest a range of behavior. Jackson and White (1989) observed that the largest normal fault ruptures consist of multiple, disjointed segments. Similarly, DuRoss et al. (2016) noted that while some of the largest historical Basin and Range province normal fault earthquakes appear to be limited to a single fault segment, others overcome fault complexity and ruptured as least parts of multiple segments.

If fault complexity were the primary reason for smaller normal fault earthquakes, we would expect to see a stronger spatial correlation between fault rupture extent and fault complexity for normal fault earthquakes compared to other fault geometries. However, this does not appear to be the case. In a study of historical earthquake fault step size—the perpendicular distance between two distinct fault traces—Wesnousky (2008) noted that both strike-slip and normal fault earthquake rupture end points correspond to fault steps approximately 70% of the time. However, normal fault earthquakes can jump larger fault steps (5 to 7 km) than strike-slip earthquakes (3 to 4 km). In a larger study, Biasi and Wesnousky (2016) also observed that normal and thrust fault earthquakes can propagate across larger fault steps than strike-slip earthquakes. They also observed that for similar length ruptures, dip-slip earthquakes (normal and thrust) include more gaps—the absence of surface rupture along an assumed continuous fault trace—than strike-slip earthquakes. Between 60% to 70% of the studied earthquake ruptures end at either a fault step or fault end, with strike-slip earthquakes more likely to end at a fault step while dip-slip earthquakes end at the fault end. For both strike-slip and dip-slip ruptures, in 30% to 40% of earthquakes the rupture ends but the fault trace continues (Biasi and Wesnousky, 2016).

Fault bends—changes in fault strike—are also thought to limit rupture extent. However, Biasi and Wesnousky (2017) found that fault bends at dip-slip rupture ends are no larger than bends within the rupture. In contrast, the ends of strike-slip ruptures corresponded to

larger bends than those within the ruptures. These results suggest that strike-slip earthquake rupture extent is more sensitive to fault bends than dip-slip earthquakes. These multiple, detailed fault rupture studies show that fault complexity limits earthquake rupture, but not that normal fault earthquakes are more sensitive to this complexity. In many cases, normal fault ruptures seem to overcome more fault complexity than strike-slip earthquakes.

Fault width, the down-dip fault extent, also impacts earthquake magnitude. As magnitude increases, so does fault width (Wells and Coppersmith, 1994). However, width is limited by the depth of the seismogenic zone (Sibson, 1986). For a given seismogenic zone depth, steeply dipping faults will have smaller widths than shallowly dipping faults. Along the San Andreas Fault, which is capable of hosting M_w 8.0 earthquakes, estimates of the seismogenic zone thickness are ~15 km (Nazareth and Hauksson, 2004), so large earthquakes can occur even for relatively thin seismogenic zones. In extensional environments, seismogenic zones are on average 10 to 15 km thick (Jackson and Blenkinsop, 1993), although some zones like the Baikal Rift have seismogenic zones more than 30 km thick (Déverchère et al., 2001). Extensional seismogenic zones are thick enough to host larger magnitude earthquakes, especially considering that most normal fault earthquakes have dips between 30° to 60° (Jackson and White, 1989; Collettini and Sibson, 2001), increasing the potential fault area within the seismogenic zone. Therefore, neither fault length nor fault width appears to limit the size of shallow continental normal fault earthquakes

9.1 Lithosphere yield stress controls M_{max}

If fault length and width are not limiting the size of continental normal fault earthquakes, then what is? Some argue that the primary energy source driving faulting differs between normal fault earthquakes and other fault geometries and may impact M_{max} (Doglioni et al., 2015; Bignami et al., 2020). Others argue that continental lithosphere may be too weak to host large normal fault earthquakes (Jackson and White, 1989). Lithosphere is weaker in extension than in compression (Sibson, 1977). Lithosphere yield-stress envelopes (also termed strength envelopes) (Figure 9), showing the difference between the most

457 compressive and least compressive principal stress axes required to induce failure,
458 illustrate that the lithosphere fails at lower stress differentials in extension than in
459 compression. Previous research also indicates a link between earthquake magnitude and
460 the lithosphere stress differential (Scholz, 2015). In laboratory experiments, Scholz (1968)
461 observed that lower stress differentials produce larger *b*-values (relatively few large
462 events) and proposed that large magnitude events occur when multiple high stress
463 asperities are linked in a rupture. Schorlemmer (2015) and Petruccelli et al. (2019) also
464 observed larger *b*-values for normal fault earthquakes and attributed them to smaller
465 stress differentials in extensional environments.
466
467 Because lithosphere is weaker in extension for both oceanic (Figure 9a) and continental
468 (Figure 9b) lithosphere, we would expect normal fault earthquakes to have a smaller M_{max}
469 in both shallow continental and oceanic environments. The lithosphere yield-stress
470 argument is compelling except that oceanic earthquakes do not appear to have the same
471 M_{max} pattern as continental earthquakes. However, a closer examination of shallow oceanic
472 normal fault earthquakes suggests that their M_{max} may actually be similar to their
473 continental brethren.
474

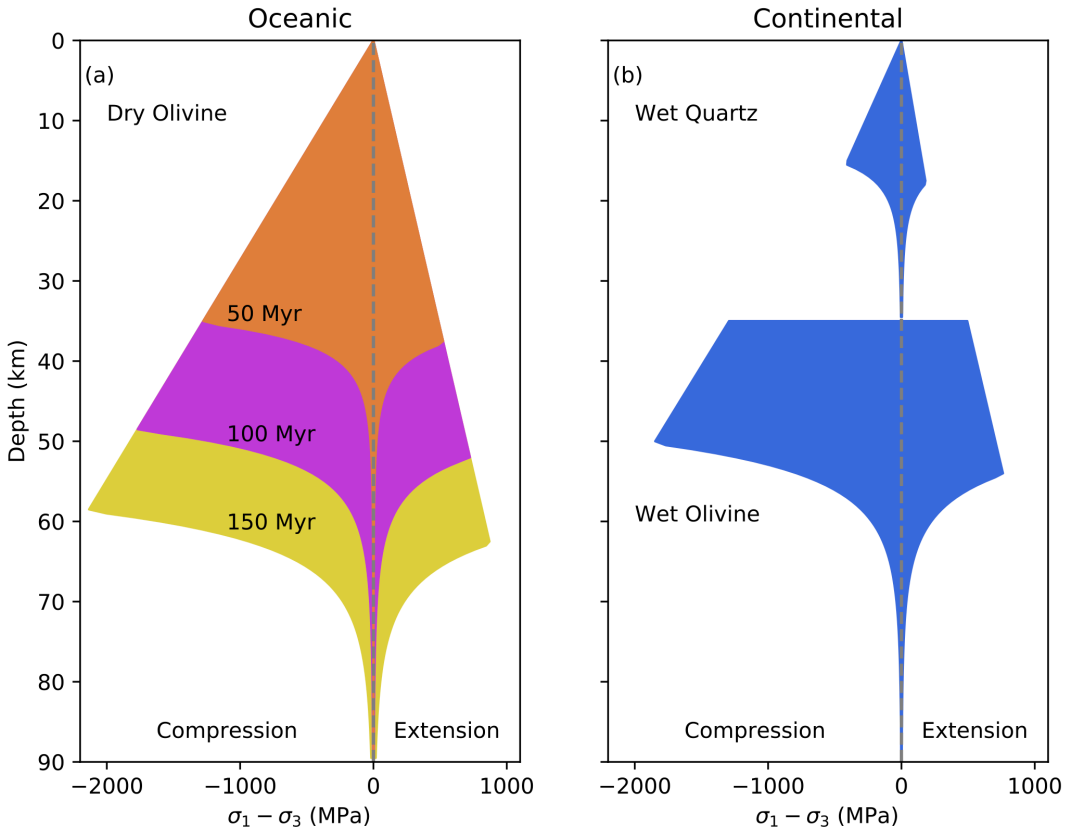

Figure 9: Yield-stress envelope (YSE) for oceanic (a) and continental (b) lithosphere in compression and extension. The oceanic YSE (a) assumes a dry olivine rheology and half-space lithosphere cooling model for 50, 100, and 150 million year-old (Myr) lithosphere. The continental YSE (b) assumes a steady-state geotherm with near-surface radioactivity. An upper wet quartz and lower wet olivine rheology are assumed. Yield stresses are higher in compression than in extension. See Appendix A for details.

As shown in Figure 1, the largest oceanic normal fault earthquakes occur between the trench and outer rise due to bending stresses in the subducting plate (Craig et al., 2014). In the GCMT catalog, these outer rise events reach ~ M_w 8, and larger ones, including the 1933 M_w 8.6 Sanriku earthquake off the coast of Japan (Kanamori, 1971), have been observed. If we remove outer rise earthquakes from the dataset, M_{max} drops as the P-axis plunge increases, as observed for continental earthquakes (Figure 10). The outlier is the 1983 Chagos earthquake, with a significant discrepancy between GCMT (M_w = 7.7) and USGS NEIC (M_w = 7.3) magnitude estimates. If the USGS NEIC M_w better reflects the true value, then shallow oceanic earthquakes away from trenches have M_{max} in the low 7 range.

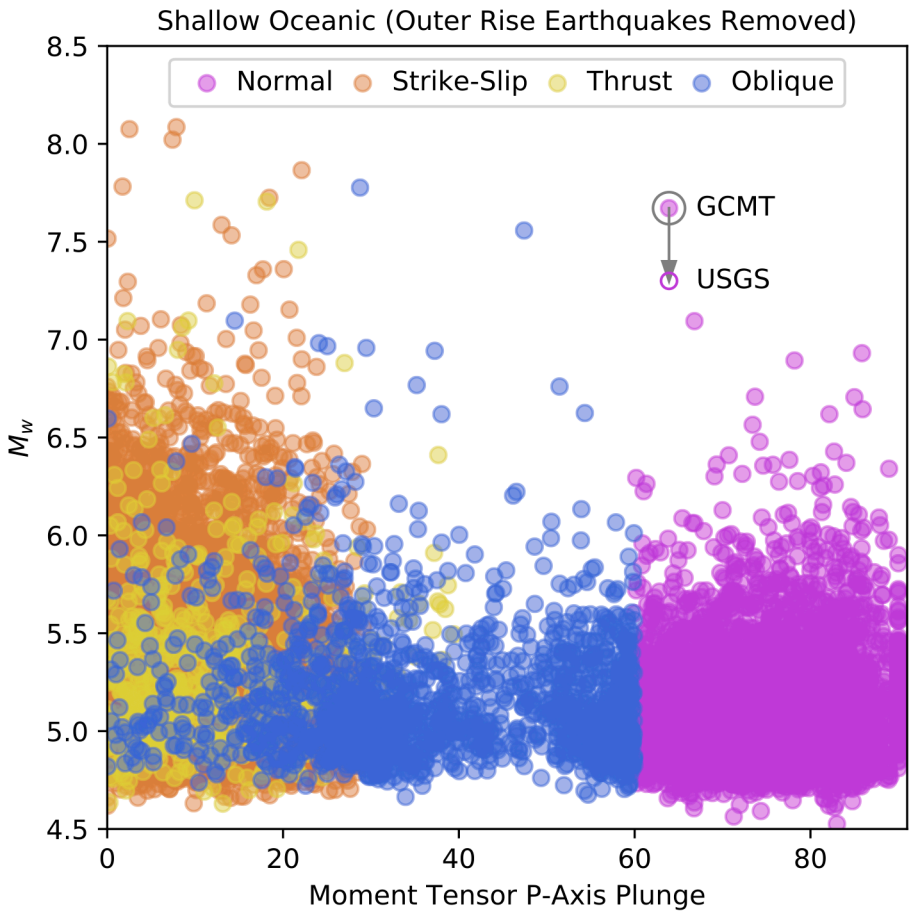

Figure 10: P-axis plunge versus moment magnitude for oceanic earthquakes with outer rise earthquakes (those earthquakes within 100 km of the trench) removed. GCMT and USGS NEIC moment magnitudes for the 1983 Chagos earthquake are indicated. With outer rise earthquakes removed, M_{max} drops as P-axis plunge increases.

Why might normal faulting earthquakes in flexural regions between the trench and outer rise have a higher M_{max} than those in extensional regions far from the trench? Perhaps this occurs because the stress fields due to plate bending differ from than those due to pure extension. For a homogenous material, pure extension produces uniform extensional stress within the material (Figure 11). Bending, however, produces extensional stress that is highest at top of the material and decreases until the neutral plane where no extensional stresses occur (Turcotte and Schubert, 2014). Below the neutral plane, the material is in

compression that increases with depth, producing thrust fault earthquakes (Craig et al., 2014).

The different stress fields may cause different failure behavior. Homogenous material fails at the same yield stress in both pure extension and bending. However, experiments (Campo, 2008; Whitney and Knight, 1980) show that materials are generally stronger in bending than in pure extension.

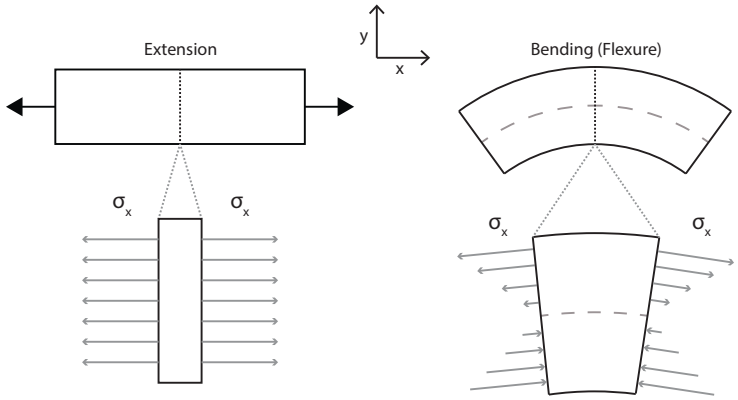

Figure 11: Schematic plot of stress within homogenous material for extension and bending. In extension, the internal stress is uniform whereas in bending the largest extensional and compressional stresses are at the outermost points.

Small defects in materials cause this strength discrepancy (Leguillon et al., 2015). In pure extension with a uniform stress field, when stress exceeds the yield stress of the weakest point, the material fails. In bending, however, stress in parts of the material may exceed the yield stress of the weakest point. Unless the weak point is near the outer surface, it will not experience the highest bending stresses. Instead, other regions will continue to experience increasing stress levels until the weak zone's yield stress is reached. When it fails, other parts of the material are actually at higher stresses.

Although the real stress state within lithosphere is complicated (Buck, 1991; Craig et al., 2014), these simple models suggest that varying yield stress may explain normal fault earthquake magnitude. In bending oceanic lithosphere, when failure occurs, the additional

areas of high stress may allow earthquakes to grow large. However, in continental lithosphere under pure extension, the yield stresses may be too low to allow large magnitude earthquakes. This reasoning follows Scholz's (1968) hypothesis that large earthquakes occur from linking several high stress asperities.

Therefore, the mode of deformation's impact on yield stress appears to be important for maximum earthquake magnitude. The weakness of lithosphere in extension appears to prevent shallow continental normal fault earthquakes from growing as large as those for other fault geometries. However, bending oceanic lithosphere's ability to produce large normal fault earthquakes indicates that fault geometry alone is an insufficient predictor of M_{max}. Understanding the lithosphere's stress state and deformation mode is thus critical in assessing a region's seismic hazard.

10.1 Conclusion

Our analysis shows that shallow continental normal fault earthquakes have a smaller maximum magnitude (in the low M_w 7 range) than other fault geometries ($\sim M_w$ 8). This maximum magnitude difference appears to be real and not an artifact of catalog length or earthquake classification. Although fault length, width, and complexity can impact the extent of an earthquake's rupture, these do not appear to be the primary reason for the smaller maximum magnitudes of shallow continental normal fault earthquakes. Instead, we propose that the weakness of lithosphere in extension is what primarily limits the size of normal fault earthquakes. The smaller maximum magnitudes of shallow continental normal fault earthquakes have important implications for seismic hazard assessment in extensional tectonic environments. In such environments, normal fault earthquakes are unlikely to exceed a low M_w 7 earthquake, even if the fault system is long enough to host much larger earthquakes.

Acknowledgments

The authors thank Northwestern University's Institute for Policy Research for supporting this research. We also thank the two anonymous reviewers for their helpful comments.

Appendix A

For the yield stress envelopes in Figure 9, we use equation 22a from Burov (2011). We use equation 12 for brittle deformation and dislocation creep (equation 15) for ductile deformation. For oceanic lithosphere we assume a dry olivine rheology. For continental lithosphere, we assume a two-layer rheology with a wet quartz crust and wet olivine mantle. We use a half-space cooling model to calculate the oceanic lithosphere and a steady-state model with shallow radioactivity for continental lithosphere—see equation 4.31 in Turcotte and Schubert (2014). Parameters used in these calculations are listed in tables A1 and A2.

Mineral/Rock	A ($MPa^{-n}s^{-1}$)	n	Q ($kJ\ mol^{-1}$)	Density (kg/m^3)
Wet Quartz	1e-4	2.4	160	2700
Wet Olivine	4.876e6	3.5	515	3300
Dry Olivine	1e4	3	520	3300

Table A1: Lithology parameters used in yield stress envelope calculations. Values from Burov (2011).

Coefficient of friction	0.5
Oceanic thermal diffusivity	0.804e-6 m^2s^{-1}
Oceanic base temperature	1330 ^oC
Oceanic surface temperature	0 ^oC
Continental surface temperature	10 ^oC
Continental mantle heat flow	30 mWm^{-2}
Length scale of radioactivity	10 km
Continental surface heat flow	56.5 mWm^{-2}
Continental thermal conductivity	3.35 $Wm^{-1}{}^oC^{-1}$
Continental crustal thickness	35 km

Table A2: Earth structure and geotherm calculation parameters.

References

Ambraseys, N. (1991) The Rukwa earthquake of 13 December 1910 in East Africa. *Terra Nova* 3(2), 202-211. doi:10.1111/j.1365-3121.1991.tb00873.x

Anderson, J.G., Biasi, G.P., Wesnousky, S.G. (2017) Fault-scaling relationships depend on the average fault-slip rate. *Bulletin of the Seismological Society of America* 107(6), 2561–2577. doi:10.1785/0120160361

Axen, G.J. (1999) Low-angle normal fault earthquakes and triggering. *Geophysical Research Letters* 26(24), 3683-3696. doi: 10.1029/1999GL005405

Ayele, A. and Kulhánek, O. (2000) Reassessment of source parameters for the three major earthquakes in the East African rift system from historical seismograms and bulletins. *Annali Di Geofisica* 43(1). 81-94. doi:10.4401/ag-3627

Biasi, G.P., Weldon, R. J., and Dawson, T. (2013) Distribution of slip in ruptures, U.S. Geol. Surv. Open-File Rept. 2013-1165, Uniform California Earthquake Rupture Forecast Version 3 (UCERF3)–The Time-Independent Model, *Appendix F*, 41 pp.

Biasi, G.P. and Wesnousky, S.G. (2016) Steps and gaps in ground ruptures: Empirical bounds on rupture propagation. *Bulletin of the Seismological Society of America* 106(3), 1110-1124. doi:10.1785/0120150175

Biasi, G.P. and Wesnousky, S.G. (2017) Bends and ends of surface ruptures. *Bulletin of the Seismological Society of America* 107(6), 2543-2560. doi: 10.1785/0120160292

Bignami, C., Valerio, E., Caminati, E., Doglioni, C., Petricca, P., Tizzani, P., and Lanari, R. (2020) Are normal fault earthquakes due to elastic rebound or gravitational collapse? *Annals for Geophysics* 63(2), SE123. doi:10.4401/ag-8455

Bilek, S.L. and Lay, T. (2018) Subduction zone megathrust earthquakes. *Geosphere* 14(4), 1468–1500. doi:10.1130/GES01608.1.

Burov, E.B. (2011) Rheology and strength of the lithosphere. *Marine and Petroleum Geology* 28, 1402-1443. doi:10.1016/j.marpetgeo.2011.05.008

Campo, E.A. (2008) Selection of Polymeric Materials: How to Select Design Properties from Different Standards, 1st ed., Published by William Andrew

Coffin, M.F., Gahagan, L.M., and Lawver, L.A. (1998) Present-day plate boundary digital data compilation. University of Texas Institute for Geophysics Technical Report No. 174.

Collettini, C. (2011) The mechanical paradox of low-angle normal faults: Current understanding and open questions. *Tectonophysics* 510(3-4), 253-268. doi:10.1016/j.tecto.2011.07.015

622 Collettini, C. and Sibson, R.H. (2001) Normal faults, normal friction? *Geology* 29(10), 927-
623 930. doi:10.1130/0091-7613(2001)029<0927:NFNF>2.0.CO;2
624
625 Craig , T.J., Copley, A., and Jackson, J. (2014) A reassessment of outer-rise seismicity and its
626 implications for the mechanics of oceanic lithosphere**.** *Geophysical Journal International*
627 197(1), 63-89. doi:10.1093/gji/ggu013

628 Dempsey, D., Ellis, S., Archer, R., and Rowland, J. (2012) Energetics of normal earthquakes
629 on dip-slip faults. *Geology* 40, 279-282. doi:10.1130/G32643.1.

630 Deng, Q.D., Sung, F.M., Zhu, S.L., Li, M.L., Wang, T.L., Zhang, W.Q., Burchfiel, B.C., Molnar, P.,
631 and Zhang, P.Z. (1984) Active faulting and tectonics of the Ningxia-Hui autonomous region,
632 China. *Journal of Geophysical Research* 89, 4427–4445. doi:10.1029/JB089iB06p04427

633 Déverchère, J., Petit, C., Gileva, N., Radziminovitch, N., Melnikova, V., and San'Kov, V. (2015)
634 Depth distribution of earthquakes in the Baikal rift system and its implications for the
635 rheology of the lithosphere. *Geophysical Journal International* 146(3), 714–730.
636 doi:10.1046/j.0956-540x.2001.1484.484.x

637 Doglioni, C., Carminati, E., Petricca, P., and Riguzzi, F. (2015) Normal fault earthquakes or
638 graviquakes. *Scientific Reports* 5**,** 12110. doi:10.1038/srep12110

639 Doser, D.I (1985) Source parameters and faulting processes of the 1959 Hebgen Lake,
640 Montana, Earthquake Sequence. *Journal of Geophysical Research* 90(B6), 4537-4555.
641 doi:10.1029/JB090iB06p04537

642 Doser, D.I. (1986) Earthquake processes in the Rainbow Mountain-Fairview Peak-Dixie
643 Valley, Nevada, region 1954–1959. *Journal of Geophysical Research* 91, 2572–2586.
644 doi:10.1029/JB091iB12p12572

645 Doser, D.I (1988) Source parameters of earthquakes in the Nevada Seismic Zone, 1915-
646 1943. *Journal of Geophysical Research* 93(B12), 15001-15015.
647 doi:10.1029/JB093iB12p15001

648 Doser, D.I. (1991) Faulting within the eastern Baikal rift as characterized by earthquake
649 studies. *Tectonophysics* 196(1-2), 109-139. doi:10.1016/0040-1951(91)90292-Z

650 Doser, D.I. and Yarwood, D.R. (1990) Strike-slip faulting in continental rifts: example from
651 Sabukia, East Africa (1928), and other regions. *Tectonophysics* 197(2-4), 213-224.
652 doi:10.1016/0040-1951(91)90042-Q

653 DuRoss, C.B., Personius, S.F., Crone, A.J., Olig S.S, Hylland, M.D., Lund, W.R., and Schwartz,
654 D.P. (2016) Fault segmentation: New concepts from the Wasatch Fault Zone, Utah, USA.
655 *Journal of Geophysical Research: Solid Earth* 121, 1131-1157. doi:10.1002/ 2015JB012519

656 Dziewonski, A.M., Chou, T.-A., and Woodhouse, J.H. (1981) Determination of earthquake
657 source parameters from waveform data for studies of global and regional seismicity.
658 *Journal of Geophysical Research: Solid Earth* 86, 2825-2852. doi:10.1029/JB086iB04p02825

659 Ekström, G., Nettles, M., and Dziewonski, A.M. (2012) The global CMT project 2004-2010:
660 Centroid-moment tensors for 13,017 earthquakes. *Physics of the Earth and Planetary*
661 *Interiors* 200-201, 1-9. doi:10.1016/j.pepi.2012.04.002

662 Frohlich, C. (1992) Triangle diagrams: ternary graphs to display similarity and diversity of
663 earthquake focal mechanisms. *Physics of the Earth and Planetary Interiors* 75(1-3), 193-
664 198. doi:10.1016/0031-9201(92)90130-N

665 Di Giacomo, D., Bondar, I., Storchak, D.A., Engdahl, E.R., Bormann, P., and Harris, J. (2015)
666 ISC-GEM: Global Instrumental Earthquake Catalog (1900-2009), III. Re-computed M_s and
667 m_b, proxy M_w, final magnitude composition and completeness assessment. *Physics of the*
668 *Earth and Planetary Interiors* 239, 33-47. doi:10.1016/j.pepi.2014.06.005

669 Gupta, H., Rao, N., Rastogi, B., and Sarkar, D. (2001) The deadliest intraplate earthquake.
670 *Science* 291(5511), 2101-2102. doi:10.1126/science.1060197
671
672 Jackson, J. and Blenkinsop, T. (1993) The Malawi earthquake of March 10, 1989: deep
673 faulting within the East African rift system. *Tectonics* 12(5), 1131-1139.
674 doi:10.1029/93TC01064
675
676 Jackson, J. and White, N.J. (1989) Normal faulting in the upper continental crust:
677 observations from regions of active extension. *Journal of Structural Geology* 11(1-2), 15-36.
678 doi:10.1016/0191-8141(89)90033-3
679
680 Johnson, K.L., Nissen, E., and Lajoie, L. (2018) Surface rupture morphology and vertical slip
681 distribution of the 1959 M_w 7.2 Hebgen Lake (Montana) earthquake from airborne LidDAR
682 topography. *Journal of Geophysical Research: Solid Earth* 123(9), 8229-8248.
683 doi:10.1029/2017JB015039

684 Kagan, Y.Y. (2002) Seismic moment distribution revisited: I. Statistical results. *Geophysical*
685 *Journal International* 148(3), 520–541. doi:10.1046/j.1365-246x.2002.01594.x

686 Kagan, Y.Y. (2003) Accuracy of modern global earthquake catalogs. *Physics of the Earth and*
687 *Planetary Interiors* 135(2–3), 173–209. doi:10.1016/S0031-9201(02)00214-5

688 Kanamori, H. (1971) Great earthquakes at island arcs and the lithosphere. *Tectonophysics*
689 12(3), 187-198. doi:10.1016/0040-1951(71)90003-5

690 Kulikova, G., and Krüger, F. (2015) Source process of the 1911 M8.0 Chon-Kemin
691 earthquake: Investigation results by analogue seismic records. *Geophysics Journal*
692 *International* 201, 1891–1911. doi:10.1093/gji/ggv091
693

694 Leguillon, D., Martin, É., and Lafarie-Frenot, M.C. (2015) Flexural vs. tensile strength in
695 brittle materials. *Comptes Rendus Mécanique* 343(4), 275-281.
696 doi:10.1016/j.crme.2015.02.003.
697
698 Manighetti, I., Caulet, C., Barros, L.D., Perrin, C., Cappa, F., and Gaudemer, Y. (2015) Generic
699 along-strike segmentation of Afar normal faults, East Africa: Implications on fault growth
700 and stress heterogeneity on seismogenic fault planes. *Geochemistry, Geophysics, Geosystems*
701 16, 443–467. doi:10.1002/2014GC005691.
702
703 Matthews, K.J., Maloney, K.T., Zahirovic, S., Williams, S.E., Seton, M., and Müller, R D. (2016)
704 Global plate boundary evolution and kinematics since the late Paleozoic. *Global and*
705 *Planetary Change* (146), 226-250. doi:10.1016/j.gloplacha.2016.10.002.
706
707 Nazareth, J.J., and Hauksson, E. (2004) The seismogenic thickness of the Southern California
708 crust. *Bulletin of the Seismological Society of America* 94(3), 940–960.
709 doi:10.1785/0120020129
710
711 Petruccelli A., Schorlemmer. D., Tormann, T., Rinaldi, A.P., Wiemer, S., Gasperini, P., and
712 Vanucci, G. (2019) The influence of faulting style on the size-distribution of global
713 earthquakes. *Earth and Planetary Science Letters* 527. doi:10.1016/j.epsl.2019.115791
714
715 Okal, E.A. (1976) Surface-wave investigation of rupture mechanism of Gobi-Altai
716 (December 4, 1957) earthquake. *Physics of the Earth and Planetary Interiors* 12, 319–328.
717 doi:10.1016/0031-9201(76)90027-3
718
719 Okal, E.A. and Romanowicz, B.A. (1994) On the variation of b-values with earthquake size.
720 *Physics of the Earth and Planetary Interiors* 87(1-2), 55-76. doi:10.1016/0031-
721 9201(94)90021-3
722
723 Okal, E.A., Synolakis, C.E., Uslu, B., Kalligeris, N., and Voukouvalas, E. (2009) The 1956
724 earthquake and tsunami in Amorgos, Greece. *Geophysical Journal International* 178(3),
725 1533-1554. doi:10.1111/j.1365-246X.2009.04237.x
726
727 Okuwaki, R. and Yagi, Y. (2017) Rupture process during the M_w 8.1 2017 Chiapas, Mexico
728 earthquake: shallow intraplate normal faulting by slab bending. *Geophysical Research*
729 *Letters* 44, 11,816–11,823. doi:10.1002/2017GL075956
730
731 Ritsema, A.R. (1974) Earthquake mechanisms of the Balkan region. *Kon. Ned. Meteor. Inst.*
732 *Repts.* 74(4), 36 pp
733
734 Rundle, J.B. (1989) Derivation of the complete Gutenberg-Richter magnitude-frequency
735 relation using the principle of scale invariance. *Journal of Geophysical Research: Solid Earth*
736 94(B9), 12337-12342. doi:10.1029/JB094iB09p12337
737
738 Scholz, C.H. (1968) The frequency-magnitude relation of microfracturing in rock and its
739 relation to earthquakes. *Bulletin of the Seismological Society of America* 58(1), 399–415.

Scholz, C.H. (2015) On the stress dependence of the earthquake *b* value. *Geophysical Research Letters* 42, 1399-1402. doi:10.1002/2014GL062863

Schorlemmer, D., Wiemer, S., and Wyss, M. (2005) Variations in earthquake-size distribution across different stress regimes. *Nature* 437(7058), 539-542. doi:10.1038/nature04094

Sibson, R.H. (1977) Fault rocks and fault mechanisms. *Journal of the Geological Society* 133(3), 191–213. doi:10.1144/gsjgs.133.3.0191

Sibson, R.H. (1986) Earthquakes and rock deformation in crustal fault zones. *Annual Review of Earth and Planetary Sciences* (14), 149-175. doi:10.1146/annurev.ea.14.050186.001053

Styron R. and Pagani, M. (2020) The GEM Global Active Faults Database (GAF-DB). *Earthquake Spectra* 36, 160-180. doi:10.1177/8755293020944182

Suter, M. (2015) Rupture of the Pitáycachi Fault in the 1887 Mw 7.5 Sonora, Mexico earthquake (southern Basin-and-Range Province): Rupture kinematics and epicenter inferred from rupture branching patterns. *Journal of Geophysical Research: Solid Earth* 120, 617–641. doi:10.1002/2014JB011244

Turcotte, D.L., and Schubert, G., 2014, *Geodynamics,* Cambridge University Press, USA.

Velasco, A.A., Ammon, C.J., Lay, T., and Hagerty, M. (1996) Rupture process of the 1990 Luzon, Philippines (Mw = 7.7), earthquake. *Journal of Geophysical Research* 101, 22,419–22,434. doi:10.1029/96JB02290

Wells, D.L. and Coppersmith, K.J. (1994) New empirical relationships among magnitude, rupture length, rupture width, rupture area, and surface displacement. *Bulletin of the Seismological Society of America* 84(4), 974–1002.

Wernicke, B. (1995) Low-angle normal faults and seismicity: A review. *Journal of Geophysical Research: Solid Earth* 100(B10), 20159– 20174. doi:10.1029/95JB01911

Wesnousky, S.G. (1988) Seismological and structural evolution of strike-slip faults. *Nature* 335, 340-343. doi:10.1038/335340a0

Wesnousky, S.G. (2008) Displacement and geometrical characteristics of earthquake surface ruptures: Issues and implications for seismic-hazard analysis and the process of earthquake rupture. *Bulletin of the Seismological Society of America* 98 (4), 1609–1632. doi:10.1785/0120070111

Whitney, J.M. and Knight, M. (1980) The relationship between tensile strength and flexure strength in fiber-reinforced composites. *Experimental Mechanics* 20, 211-216.

786 Yu, G., Xu, X., Klinger, Y., Diao, G., Chen, G., Feng, X., Li, C., Zhu, A., Yuan, R., Guo, T., Sun, X. et
787 al. (2010) Fault-scarp features and cascading-rupture model for the Mw 7.9 Wenchuan
788 earthquake, eastern Tibetan plateau, China. *Bulletin of the Seismological Society of America*
789 100, 2590–2614. doi:10.1785/0120090255